

A TEMPORARY EPOCH OF STALLED SPIN-DOWN FOR LOW-MASS STARS:
INSIGHTS FROM NGC 6811 WITH *Gaia* AND *Kepler*

JASON LEE CURTIS,^{1,*} MARCEL A. AGÜEROS,¹ STEPHANIE T. DOUGLAS,^{2,*} AND SØREN MEIBOM²

¹*Department of Astronomy, Columbia University, 550 West 120th Street, New York, NY 10027, USA*

²*Center for Astrophysics | Harvard & Smithsonian, 60 Garden Street, Cambridge, MA 02138, USA*

(Accepted May 16, 2018)

Submitted to *The Astrophysical Journal*

ABSTRACT

Stellar rotation was proposed as a potential age diagnostic that is precise, simple, and applicable to a broad range of low-mass stars ($\leq 1 M_{\odot}$). Unfortunately, rotation period (P_{rot}) measurements of low-mass members of open clusters have undermined the idea that stars spin down with a common age dependence (i.e., $P_{\text{rot}} \propto \sqrt{\text{age}}$): K dwarfs appear to spin down more slowly than F and G dwarfs. Agüeros et al. (2018) interpreted data for the ≈ 1.4 -Gyr-old cluster NGC 752 differently, proposing that after having converged onto a slow-rotating sequence in their first 600–700 Myr (by the age of Praesepe), K dwarf P_{rot} stall on that sequence for an extended period of time. We use data from *Gaia* DR2 to identify likely single-star members of the ≈ 1 -Gyr-old cluster NGC 6811 with *Kepler* light curves. We measure P_{rot} for 171 members, more than doubling the sample relative to the existing catalog and extending the mass limit from ≈ 0.8 to $\approx 0.6 M_{\odot}$. We then apply a gyrochronology formula calibrated with Praesepe and the Sun to 27 single G dwarfs in NGC 6811 to derive a precise gyrochronological age for the cluster of 1.04 ± 0.07 Gyr. However, when our new low-mass rotators are included, NGC 6811’s color– P_{rot} sequence deviates away from the naive 1 Gyr projection down to $T_{\text{eff}} \approx 4295$ K (K5V, $0.7 M_{\odot}$), where it clearly overlaps with Praesepe’s. Combining these data with P_{rot} for other clusters, we conclude that the assumption that mass and age are separable dependencies is invalid. Furthermore, the cluster data show definitively that stars experience a temporary epoch of reduced braking efficiency where P_{rot} stall, and that the duration of this epoch lasts longer for lower-mass stars.

Keywords: open clusters: individual (NGC 6811, Pleiades, Praesepe) — stars: evolution — stars: rotation — stars: solar-type

1. INTRODUCTION

Sun-like stars change very little over their main-sequence lifetimes, making their ages one of their most challenging properties to determine. However, knowing stellar ages, especially for low-mass stars ($\leq 1 M_{\odot}$), is essential in this era of precision astrophysics. On the Galactic scale, our current inability to provide confident ages for these stars limits our understanding of the Milky Way’s star-formation history and chemical enrichment. On the planetary-system scale, it nega-

tively impacts the development of theories for planet formation and evolution.

Forty-seven years ago, Skumanich (1972) compared rotation for solar-mass members of young nearby clusters (the Pleiades, Ursa Major, and the Hyades) to the Sun, and noted that stars appeared to spin down according to the square-root of age, which has since become known as the Skumanich Law. Barnes (2003) built on this work to propose the use of rotation periods (P_{rot}) as a clock, which he termed gyrochronology. A reliable rotation–age relation would be a boon to the study of these stars, because other techniques for obtaining their ages generally do not work (Soderblom 2010). For example, for K and M stars, relying on evolution off of the zero-age main-sequence and the subsequent increase in

Corresponding author: Jason Lee Curtis
jasoncurtis.astro@gmail.com

* NSF Astronomy and Astrophysics Postdoctoral Fellow

luminosity or decrease in surface gravity cannot lead to meaningful constraints on ages, as these parameters are practically unchanged over the age of the Universe.

Unfortunately, observational efforts to constrain the rotation–age relation, based largely on observations of open clusters, have made our hopes for a simple relation fade. For example, when comparing the color– P_{rot} distributions for M35 (150 Myr) and M34 (220 Myr) to that for the Hyades (727 Myr¹), Meibom et al. (2009, 2011a) found that while the F and G dwarfs had spun down following the Skumanich Law, K-type Hyads appeared to rotate too rapidly relative to their younger counterparts in M35 and M34, after projecting each sample to a common age using $P_{\text{rot}} \propto t^{0.5}$. Meibom et al. (2011b) noted a similar behavior for the early K dwarfs in NGC 6811 (1 Gyr). Cargile et al. (2014) reached a similar conclusion upon comparing rotation data for Blanco 1 (132 Myr; Cargile et al. 2010) to these same clusters. These authors suggested that Sun-like FGK dwarfs spin down continuously, but with time dependencies that differ according to mass.

Barnes (2007, 2003) derived gyrochronology relations that decoupled the mass and age dependence of stellar spin-down. Any mass dependence could then be determined from the P_{rot} sequences observed in young, nearby clusters, and the age index n , also known as the braking index, for the t^n power law could be fitted for by comparing those sequences to the Sun’s P_{rot} and age.

However, while re-tuning the coefficients for the Barnes (2007) gyrochronology equation, Angus et al. (2015) were forced to discard data for Praesepe (670 Myr) and NGC 6811. In addition, Agüeros et al. (2018) analyzed light curves from the Palomar Transient Factory (PTF; Law et al. 2009; Rau et al. 2009) for the ≈ 1.4 -Gyr-old² cluster NGC 752 and found that the cluster’s early K dwarfs had barely slowed relative to Praesepe’s, while the late K and early M dwarfs had not spun down at all, despite being about twice as old.

Here, we re-examine rotation in the 1 Gyr cluster NGC 6811. We use high-precision astrometry and photometry from *Gaia* to identify cluster members with *Kepler* light curves, which extends the 1-Gyr rotator sample from $\approx 0.8 M_{\odot}$ (Meibom et al. 2011b) down to $\approx 0.6 M_{\odot}$ (Section 2). Next, we compare our expanded sample to the rotation data for the younger cluster Praesepe, and

show that while the F and G dwarfs have spun down as expected, the K dwarfs have not slowed at all in the intervening ≈ 350 Myr. Finally, we demonstrate that this cannot be due to K dwarfs simply spinning down more slowly than F/G dwarfs, but instead must be caused by a temporary period of stalled braking (Section 3). We conclude in Section 4.

2. NEW ROTATORS IN NGC 6811

Below, we review the properties of NGC 6811, first observed by John Herschel in 1829 (Herschel 1833). We then expand the cluster’s membership with data from the second *Gaia* data release (DR2; Gaia Collaboration et al. 2018a) and determine the properties of these stars. We also discuss the rotation results from Meibom et al. (2011b) before measuring P_{rot} for those stars with *Kepler* (Basri et al. 2005) light curves and producing a new color– P_{rot} distribution for the cluster.

2.1. The age, metallicity, and reddening of NGC 6811

Sandquist et al. (2016) presented a thorough analysis of NGC 6811, including the characterization of a detached partially eclipsing binary (EB), measurements of asteroseismic parameters for helium-burning giants, study of the pulsating stars at the main-sequence turnoff, and an analysis of its color–magnitude diagram (CMD). While there is some tension between the age solutions for the two EB components, most of the data support an age for the cluster of 1 ± 0.05 Gyr (Sandquist et al. 2016), in agreement with the Janes et al. (2013) *UBVRI* photometric analysis.

Sandquist et al. (2016) also summarized the spectroscopic metallicity measurements in the literature from various sources, which agree on an approximately solar metallicity with values ranging from -0.02 to $+0.04$ dex. Finally, Sandquist et al. (2016) found an interstellar reddening value of $E(B-V) = 0.07 \pm 0.02$ (corresponding to $A_V = 0.22$), while various literature values range from $E(B-V) = 0.05$ to 0.14 ($A_V = 0.16$ to 0.43). This is consistent with the 3D dust map value built with Pan-STARRS 1 and 2MASS photometry, which estimates $A_V = 0.25 \pm 0.06$ at 1.15 kpc (Green et al. 2018).³ In Section 3.1, we refine the reddening/extinction value by fitting a gyrochronology model to the color–period distribution and find $A_V = 0.15$.

2.2. Identifying NGC 6811 members with *Gaia*

The Meibom et al. (2011b) study of rotation in NGC 6811 relied on a sample vetted with radial velocities (RVs) to clean the *Kepler* ($g-r$)_{KIC} vs. g _{KIC} CMD.

¹ Douglas et al. (2019) calculated a differential gyrochronology age of 727 Myr for the Hyades relative to Praesepe, which we fixed to 670 Myr based on the median of several literature isochrone ages.

² Agüeros et al. (2018) inferred an age of 1.34 Gyr for NGC 752; Anthony-Twarog et al. (2014) found 1.45 Gyr. We average the two results and round it to 1.4 Gyr.

³ <http://argonaut.skymaps.info>

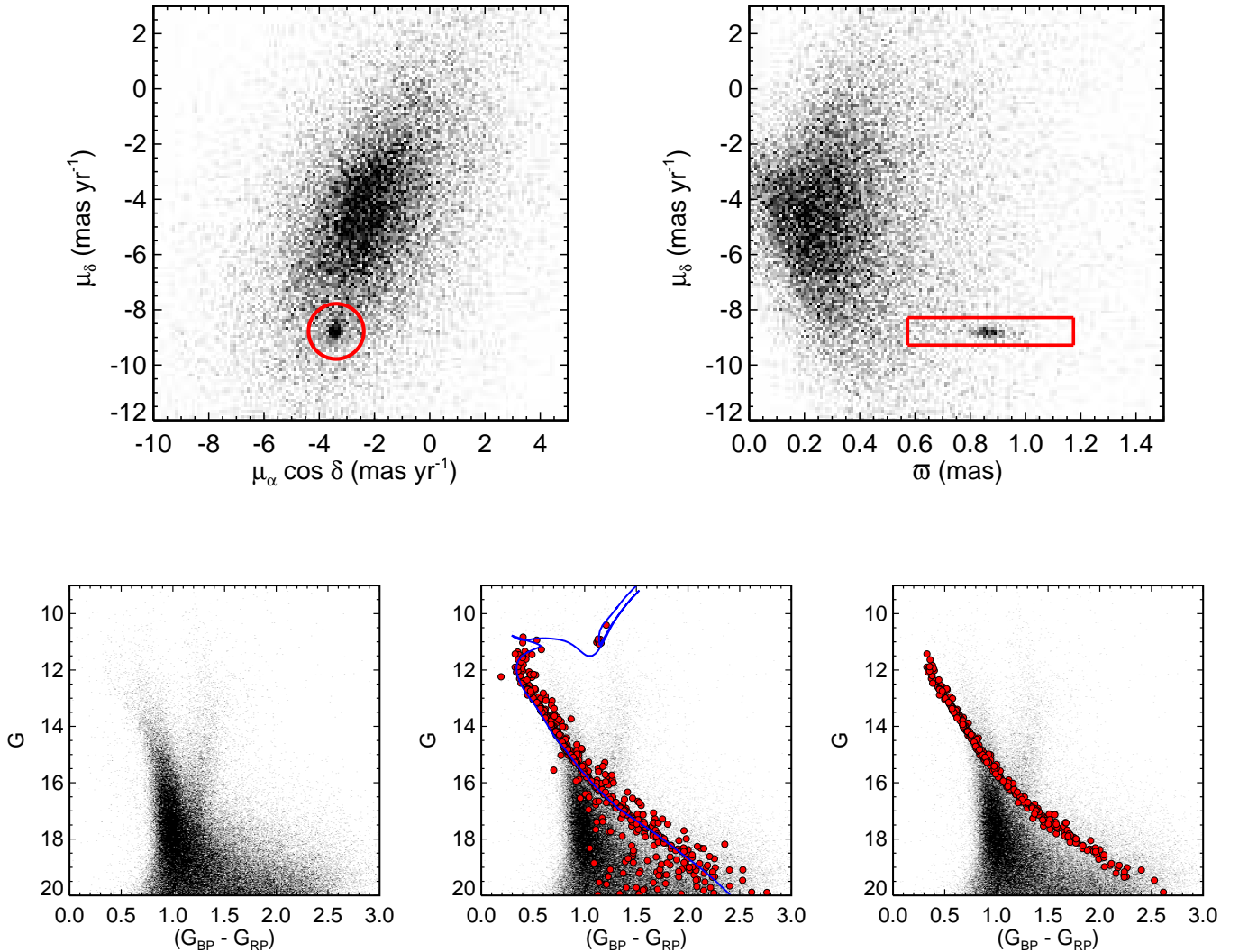


Figure 1. Selection of single-star members of NGC 6811 with *Gaia* DR2. *Top left*—Proper motions of stars within 1° of NGC 6811 and $G < 18$ mag (we considered stars with $G < 20$; we adjust this threshold for clarity in this figure); the red circle has a radius of 1 mas yr^{-1} , which is double the value we adopted for membership criteria (0.5 mas yr^{-1}) to make this panel easier to view. *Top right*—Parallax versus declination proper motion for the same stars. The red box shows our selection criteria (0.3 mas in parallax, and again 0.5 mas yr^{-1} in proper motion). *Bottom left*—The CMD for the $\approx 87,000$ stars in the field. *Bottom middle*—The 485 stars satisfying our astrometric criteria are highlighted in red. A 1 Gyr PARSEC model with solar composition, $A_V = 0.15$, and $(m - M) = 10.2$ is overlaid in blue. *Bottom right*—The subset of 322 astrometric (unevolved) members that follow the cluster’s single-star sequence are highlighted in red.

Gaia recently delivered high-precision astrometry (positions, proper motions, parallaxes) and photometry (G , G_{BP} , G_{RP}) for $> 1.3 \times 10^9$ stars (Gaia Collaboration et al. 2018a). These data greatly simplify the process of identifying single-star members of open clusters (e.g., Gaia Collaboration et al. 2018b).

We determine the cluster’s DR2 proper motion (μ) and parallax (ϖ) from the 71 members identified by Meibom et al. (2011b): $\mu_\alpha \cos \delta = -3.39 \text{ mas yr}^{-1}$,

$\mu_\delta = -8.78 \text{ mas yr}^{-1}$, and $\varpi = 0.87 \text{ mas}$. There are 86,853 stars within 1° of NGC 6811’s center (a 19 pc search radius at $d = 1096 \text{ pc}$)⁴ in DR2 with $G < 20$ mag and usable astrometry and photometry, but only 485 satisfy our simple astrometric criteria: μ within

⁴ $(\alpha, \delta) = 19^{\text{h}} 37^{\text{m}} 12^{\text{s}}, +46^\circ 23' 15''$.

0.5 mas yr⁻¹ and ϖ within 0.3 mas of the median for these 71 stars (see top row of Figure 1).

After applying our astrometric cuts, we overplot the candidate cluster members on the *Gaia* CMD for the region around NGC 6811. (see the bottom row of Figure 1). The cluster’s CMD is visually well-fit with a PARSEC isochrone model (Bressan et al. 2012; Chen et al. 2014) for an age of 1 Gyr, solar composition, $A_V = 0.15$, and $(m - M) = 10.2$, as shown in the bottom middle panel of Figure 1.

We then use the Hyades main-sequence from Gaia Collaboration et al. (2018b) to define an empirical single-star sequence, which we fit with a cubic basis spline to predict M_G from $(G_{BP} - G_{RP})$. Next, we apply the Hyades model to the NGC 6811 astrometric candidates using the NGC 6811 extinction and distance modulus, and filter out stars that are offset by more than 0.5 mag in M_G from the model.

We fit a cubic basis spline to the stars remaining in the NGC 6811 sample to define the cluster’s single-star sequence more accurately, and then re-extract the single stars with a stricter cut of 0.25 mag. In this manner, we identify 322 likely single members along the main-sequence of NGC 6811 (see bottom right panel of Figure 1). While this is not a complete census of the cluster’s membership, this new catalog is all that is required for this work, which focuses on the rotational behavior of single stars.⁵

2.3. Determining stellar properties

While the DR2 stellar properties pipeline (Apsis; Bailer-Jones et al. 2013; Andrae et al. 2018) produced effective temperatures (T_{eff}) from the DR2 photometry for 1.61×10^8 stars with $G < 17$ mag and $3000 < T_{\text{eff}} < 10,000$ K, these notably do not incorporate the effects of reddening. We therefore generate a color- T_{eff} relation using three separate catalogs of precisely characterized nearby stars: the Brewer et al. (2016) sample of FGK stars observed by the California Planet Search with Keck/HIRES, the Boyajian et al. (2012) sample of K and M dwarfs with interferometric radii and bolometric fluxes, and the Mann et al. (2015) M dwarfs characterized with optical and near-infrared

spectroscopy. Deriving our own empirical relation also allows us to correct for NGC 6811’s metallicity.⁶

The temperatures of stars hotter than 4100 K in our benchmark sample are consistent with the DR2 values to within 70 K (root-mean-square error), with most of the remaining scatter due to the $(G_{BP} - G_{RP})$ color’s dependence on metallicity along with T_{eff} (see figure 2 of Morris et al. 2018). However, the Apsis T_{eff} values diverge from those in our sample for $T_{\text{eff}} < 4100$ K.

We also translate our photometric T_{eff} values to spectral types (SpT) and stellar masses (M_\star) using the Kraus & Hillenbrand (2007) stellar spectral energy distribution table (their table 5) to aid the reader’s interpretation of our results. We interpolate mass from T_{eff} , but only quote the SpT at the nearest T_{eff} entry in the Kraus & Hillenbrand (2007) table, which for our sample includes the following spectral types: F5, F8, G0, G2, G5, G8, K0, K2, K4, K5, K7, M0, and M1. Our T_{eff} , M_\star , and SpT values are listed in Table 1 for all the rotators we identify below and use in our analysis.

2.4. Revisiting the Meibom et al. (2011b) results

NGC 6811 was observed during the primary *Kepler* mission. Meibom et al. (2011b) presented rotation periods measured from light curves for Quarters 1-4 for the 71 members they confirmed by RV monitoring.

Two of these stars appear to rotate too slowly in the color- P_{rot} plot for NGC 6811: KICs 9595724 and 9717386. These stars are also outliers in the cluster’s DR2 proper motion diagram, and appear too bright in the DR2 CMD, which indicates that they are either not members or are binaries. Either way, they should be removed from the gyrochronology calibration sample.

KIC 9594645 also has a discrepant proper motion (by 1 mas yr⁻¹), and appears fainter than the cluster’s single-star sequence. Although its P_{rot} is consistent with the cluster distribution, we reclassify it as a non-single-member and remove it from our sample.

We identified five other photometric binaries in the DR2 CMD (KICs 9594100, 9655310, 9471038, 9775381, 9592939). While they are consistent with the cluster color- P_{rot} distribution, that distribution is well populated, and we opted to remove these from the sample.

Figure 2 shows the CMD and color- P_{rot} diagram for the Meibom et al. (2011b) sample of 71 stars, and highlights the eight stars we identified as non-single-members

⁵ While characterizing the binary population is critical in any cluster, in this context binaries are contaminants. Binary companions may exert tidal or other physical effects on the primary star (e.g., Meibom & Mathieu 2005; Meibom et al. 2007; Douglas et al. 2016, 2017), causing us to locate stars incorrectly in the color- P_{rot} plane, and leading us to misidentify trends or transitions in the period distribution.

⁶ Throughout this work, we use the DR2 extinction coefficients from the Evans et al. (2018) passbands provided by the PARSEC isochrone web page (http://stev.oapd.inaf.it/cgi-bin/cmd_3.0) for a G2V star using the Cardelli et al. (1989) extinction law with $R_V = 3.1$, where $E(G_{BP} - G_{RP})/A_V \approx 0.416$ and $A_G/A_V \approx 0.859$, and ignore their dependence on spectral type.

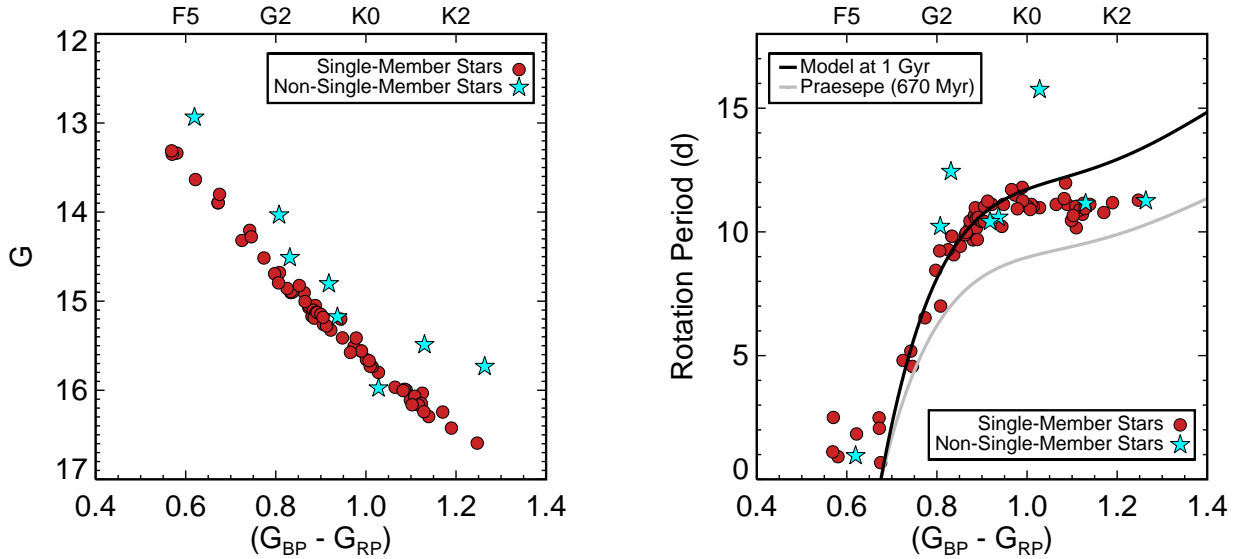


Figure 2. CMD (*left*) and color–period diagram (*right*) for the 71 stars in the Meibom et al. (2011b) rotator sample for NGC 6811. We identified eight photometric and proper motion outliers (cyan stars), two of which are also outliers in the color–period diagram. A 1 Gyr gyrochronology model (upper black line), calibrated from fitting the Praesepe color–period sequence (lower gray line) and tuned with the Sun, is also included. This model, with braking index $n = 0.62$, fits the F and early-G dwarfs, but diverges from the later-G and K dwarfs.

according to DR2. This leaves 63 stars in the Meibom et al. (2011b) sample with masses $0.79 < M_{\star} < 1.29 M_{\odot}$ (K2V to F5V).

2.5. Measuring P_{rot} with *Kepler* (again)

We search the Mikulski Archive for Space Telescopes⁷ for *Kepler* data for the 278 stars we identify as NGC 6811 members with $(G_{\text{BP}} - G_{\text{RP}}) \gtrsim 0.57$ (the bluest published rotator; Meibom et al. 2011b). We find light curves for 203 stars, 62 of which are redder than the Meibom et al. (2011b) sample. We analyze the pre-search data conditioning simple aperture photometry (PDC-SAP; Stumpe et al. 2012; Smith et al. 2012) light curves from Quarters 2–16. Quarters 1 and 17 were truncated and only lasted for 33.47 d and 31.75 d, respectively, whereas the intervening Quarters covered ≈ 90 d, except for Quarter 8, which lasted for ≈ 67 d. Most stars have more than one quarter of data.

We compute Lomb–Scargle periodograms (Scargle 1982; Press & Rybicki 1989) for all available quarters for each star (see Figure 3 for an example of our analysis), and report the median and standard deviation values for the resulting P_{rot} in Table 1. Occasionally, the peak power in the periodogram corresponds to a half-period harmonic (9% of the total number of all P_{rot} measurements). We automatically detect these cases by

identifying outliers with values that when doubled were within 10% of the median value from all quarters, then correct the measured P_{rot} by doubling their values.

McQuillan et al. (2014) reported P_{rot} for 87 of our stars, 57 of which were not identified as members by Meibom et al. (2011b). In Figure 4, we compare the P_{rot} values we find to those in both Meibom et al. (2011b) and McQuillan et al. (2014), and find close agreement. For McQuillan et al. (2014), we calculate the differences from our periods and find no net offset and a standard deviation of only $\sigma = 0.15$ d.

Finally, there are 11 stars with multi-quarter data with large standard deviations; $\sigma_{P_{\text{rot}}} > 1$ d. We discard these from our sample and attribute them to limitations in the data quality or perhaps blending of stars in the *Kepler* photometric apertures. Our measurements are displayed in a color– P_{rot} diagram in Figure 5. Table 1 lists the 171 candidate single-star members that now have a measured P_{rot} , and includes 10 stars that are period outliers (they appear too fast or too slow relative to the cluster color– P_{rot} sequence, which we expect to be fully and tightly converged since the distributions for Praesepe and the Hyades are, as demonstrated by Douglas et al. 2019). The remaining 161 rotators more than double the size of the Meibom et al. (2011b) sample and extend it to $\approx 0.6 M_{\odot}$.

⁷ <https://archive.stsci.edu>

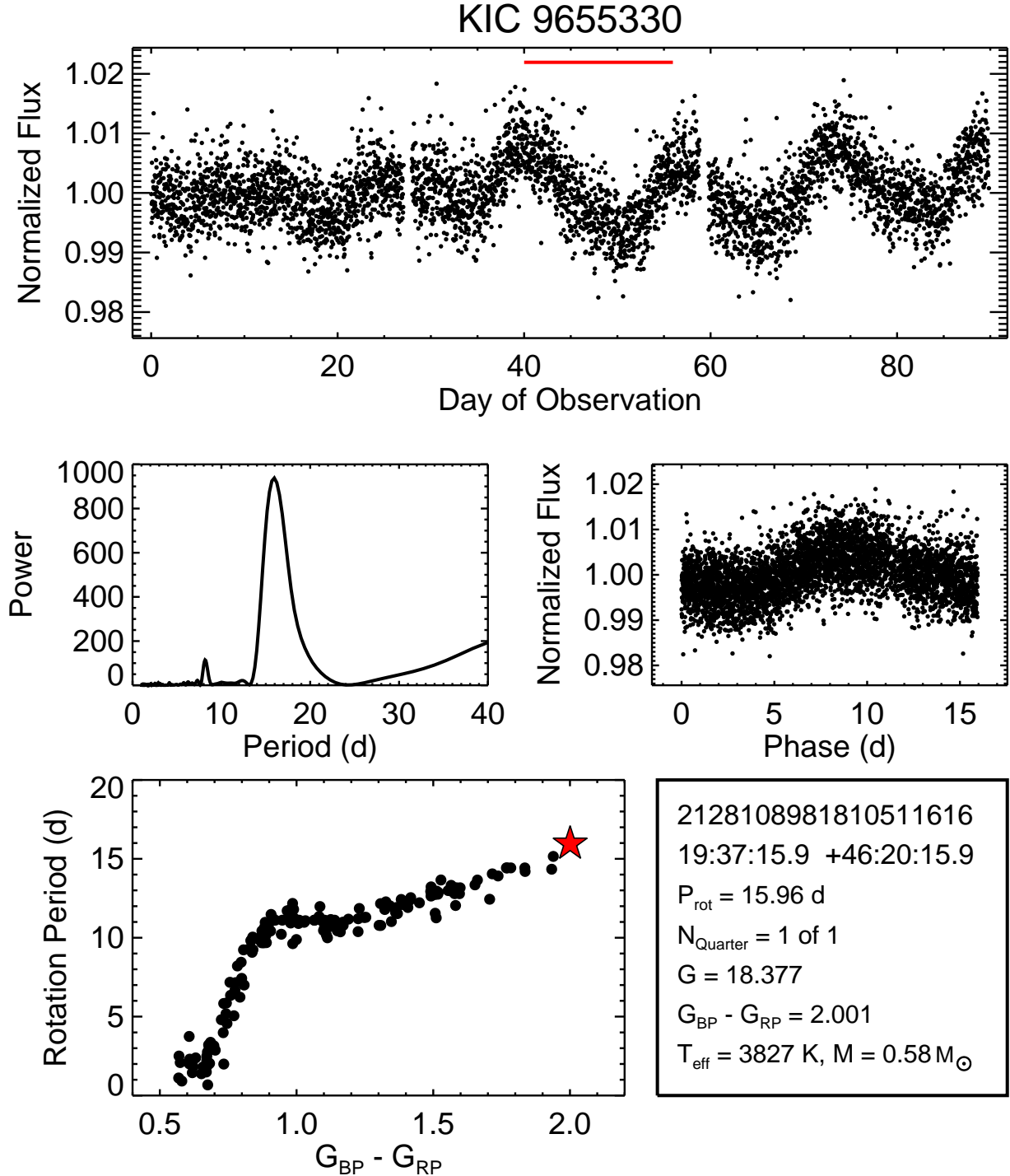


Figure 3. Analysis of the *Kepler* light curve for KIC 9655330 (Gaia DR2 2128108981810511616), the faintest, reddest, and slowest star in our sample. *Top*—The Quarter 6 *Kepler* PDCSAP light curve for this target. The length of the red line at the top left is the duration of one cycle (i.e., P_{rot}). This is the only available *Kepler* light curve for this star. *Middle left*—The Lomb–Scargle periodogram for the light curve peaks at $P_{rot} = 15.96$ d. *Middle right*—The phase-folded light curve shows a clean repeating pattern. *Bottom left*—The color–period diagram for NGC 6811 with this star highlighted (red star). *Bottom right*—Reference information for this star, including Gaia DR2 Source ID, coordinates, P_{rot} (and the standard deviation of values when multiple quarters are available), the number of quarters used to calculate P_{rot} , G magnitude and $(G_{BP} - G_{RP})$ color, and estimates for T_{eff} and mass. Versions of this figure panel for every target analyzed (171 images) are available as an electronic figure set in the online Journal.

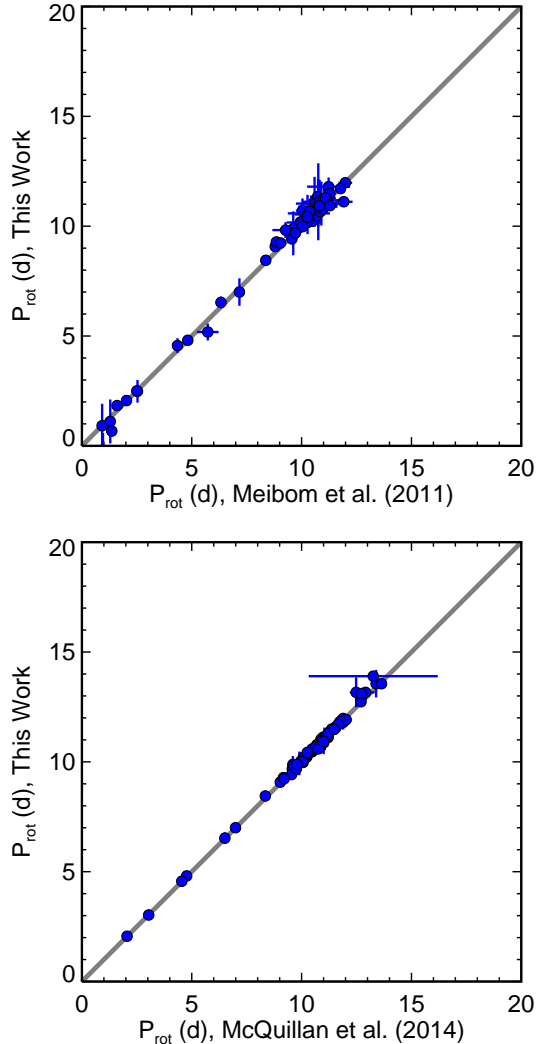


Figure 4. Comparison between our measured periods and values from (*top*) Meibom et al. (2011b) and (*bottom*) McQuillan et al. (2014) for these same stars. Our measurements show excellent agreement with previous ones.

3. DISCUSSION

Below, we calculate the reddening and age for NGC 6811 using gyrochronology. Next, we show that the NGC 6811 K dwarfs have not spun down relative to their cousins in Praesepe, despite their large difference in age. Finally, we present evidence supporting the scenario whereby stars stop spinning down, effectively stalling in their angular-momentum evolution, for an extended period of time.

3.1. A gyrochronology reddening and age for NGC 6811 using *F* and *G* members

In addition to the P_{rot} distribution for NGC 6811, Figures 2 and 5 include information on the rotational

properties of younger stars in Praesepe. In each figure, the lower gray line corresponds to the Douglas et al. (2019) fit to Praesepe’s slowly rotating sequence. These authors constructed a gyrochronology model using these data as a first epoch (670 Myr, $A_V = 0.035$), and the Sun as a second epoch (4.567 Gyr, $(G_{\text{BP}} - G_{\text{RP}})_{\odot} = 0.82$), and derive a braking index $n = 0.62$.⁸ The second, higher gray line in each figure projects their fit from 670 Myr to 1 Gyr using this new braking index.

Inspecting the color– P_{rot} sequence for NGC 6811 and the fit to Praesepe data shown in Figure 5, it is clear that the F and G stars in Praesepe (which sit on the lower gray line) have spun down by the age of NGC 6811. This means that we can use these stars to obtain an age for NGC 6811, as long as our gyrochronology model takes Praesepe as its first epoch.

Reddening is an important ingredient in a gyrochronology age calculation. The rapid rise in F dwarf P_{rot} over the narrow range in T_{eff} seen in Figure 5 (which corresponds to $0.65 < (G_{\text{BP}} - G_{\text{RP}})_0 < 0.75$, where $(G_{\text{BP}} - G_{\text{RP}})_0$ is the unreddened color; see Figure 6) provides a tight constraint on reddening that is relatively insensitive to age. We fit for reddening by comparing the color– P_{rot} sequences for Praesepe and NGC 6811. To account for Praesepe’s uncertain age, we re-model the un-reddened Praesepe sequence with a sixth order polynomial, $A_V = 0.035$ and ages $t = 650$ and 700 Myr, and re-calculate the braking index relative to the Sun, finding $n = 0.61$ and 0.63 for the two ages.

We project our Praesepe model forward to 1 Gyr, the isochrone age of NGC 6811, and minimize χ^2 between our measured P_{rot} and the model predictions for the 16 members with $0.65 < (G_{\text{BP}} - G_{\text{RP}})_0 < 0.75$. We repeat this exercise for ages of 0.9 and 1.1 Gyr to constrain the age sensitivity on reddening, and find $A_V = 0.156^{+0.016}_{-0.020}$ and $A_V = 0.145^{+0.018}_{-0.023}$, for $E(B - V) = 0.050^{+0.005}_{-0.006}$ and $E(B - V) = 0.047^{+0.006}_{-0.007}$, for the 650 and 700 Myr cases respectively. The exact ages for Praesepe and NGC 6811 only have a small impact on the resulting reddening, as we illustrate in Figure 6.

Indeed, even adopting an 800 Myr age for Praesepe (Brandt & Huang 2015), the braking index increases to $n = 0.68$, the gyrochronology age for NGC 6811 increases to 1.2 Gyr, but we still find the same reddening value. However, this age is inconsistent with the cluster CMD. A 1.2 Gyr PARSEC isochrone with solar metallicity can only be approximately fit to the cluster turnover

⁸ According to models by van Saders & Pinsonneault (2013), metallicity is not expected to significantly impact angular momentum evolution when period distributions are analyzed with respect to temperature (and therefore color) instead of mass.

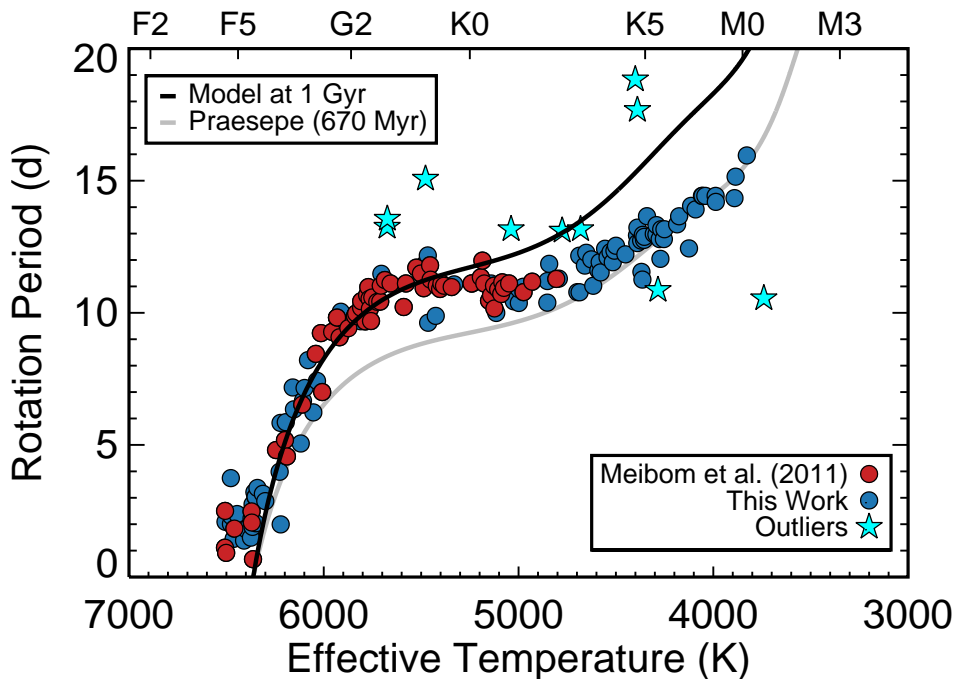


Figure 5. The effective temperature–period distribution for 171 members of NGC 6811. The 63 red-shaded points are from Meibom et al. (2011b), and the 10 cyan stars mark outliers with periods deviating from the main trend by more than 2 d. Our expanded sample more than doubles the number of known rotators and extends their mass range from $0.8 M_{\odot}$ to $0.6 M_{\odot}$ (blue points). We compare the NGC 6811 period sequence to a fit to Praesepe (lower line), which we also evolved forward to 1 Gyr with $n = 0.62$. Stars with $T_{\text{eff}} > 5400$ K have all spun down relative to Praesepe following this model, but the sequence flattens out toward cooler temperatures, diverging from the NGC 6811-age model (upper line) and continuing toward the Praesepe sequence. The stalling of spin-down is now very clear: the lowest mass stars in NGC 6811 seem to be spinning at the same rates as their younger cousins in Praesepe.

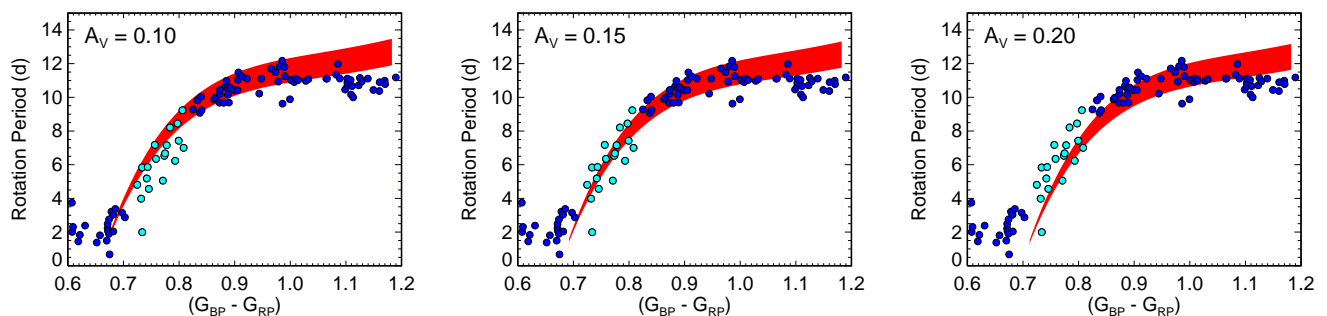


Figure 6. Interstellar reddening can be precisely constrained from the color–period diagram of a cluster with an approximately known age. The NGC 6811 color–period diagram is shown in all three panels, and the F dwarfs are highlighted (cyan points). Gyrochronology models built with Praesepe and the Sun ($n = 0.61$) with ages ranging from 0.9 to 1.1 Gyr are shaded in red, with extinction values applied of $A_V = 0.10$ (left), 0.15 (middle), and 0.20 (right). The location of the F dwarf sequence is more sensitive to reddening than to age. Fitting our Praesepe-derived model to NGC 6811, we find $A_V = 0.15 \pm 0.02$, where the uncertainty comes from varying Praesepe’s age between 650 and 700 Myr and NGC 6811’s age between 0.9 and 1.1 Gyr.

by reducing the reddening to zero. This is inconsistent with expectations from the 3D dust map (Green et al. 2018), which has $A_V = 0.25 \pm 0.06$ at the location and distance of NGC 6811. That value is larger than our result. However, if $A_V = 0.25$, we would then infer an age of 1.26 Gyr with our gyrochronology model, but then a CMD isochrone analysis would demand a significantly younger age of ≈ 0.95 Gyr. The only reddening and age combination that gives a precise and consistent match between isochrone and gyrochronology models with the data is our solution of $A_V = 0.15$ and 1 Gyr. We use $A_V = 0.15$ for the remainder of this work.

To calculate the cluster age, we consider only G dwarfs with $0.75 < (G_{BP} - G_{RP})_0 < 0.90$ (29 stars within $5500 < T_{\text{eff}} < 6000$ K) by applying $A_V = 0.15$. While we do demonstrate in this paper that gyrochronology fails to describe K dwarf spin-down, Meibom et al. (2015) showed that gyrochronology does accurately represent G dwarfs at 2.5 Gyr and van Saders et al. (2016) showed that it remains valid up to the age of the Sun. We chose our color cutoff by inspecting where the model diverges from the data in Figure 5, corresponding to $T_{\text{eff}} \approx 5400$ K. We find a gyrochronological age of $t_{\text{gyro}} = 1.04 \pm 0.12$ Gyr (median and standard deviation) if Praesepe is 670 Myr old (the age derived from an analysis of literature ages by Douglas et al. (2019)). Trimming the outliers shown in Figure 5 (two of the cyan stars) reduces the standard deviation to 75 Myr or $\approx 9\%$, which is incredibly precise. The standard deviation of the mean is only $\approx 1.5\%$. This gyrochronology age is consistent with the literature isochrone ages (Sandquist et al. 2016; Janes et al. 2013).

As a final test, we solve for reddening and age simultaneously. We minimize χ^2 by brute force with both properties as free parameters and find an age of 1.00 Gyr and $A_V = 0.15$, consistent with our previous results.

3.2. Further evidence for a temporary epoch of stalled spin-down for K stars

The Meibom et al. (2011b) color- P_{rot} sequence for NGC 6811 (Figure 2) seems oddly flat compared to that for other clusters and to model expectations: all of the stars less massive than $M_{\star} \lesssim 1 M_{\odot}$ appear to have the same P_{rot} . Meibom et al. (2011b) noted that extrapolating a younger cluster forward in age with the Skumanich Law predicts a different, more sloped shape to this sequence, with lower-mass stars rotating more slowly than their more massive neighbors in color- P_{rot} space.

Our work confirms NGC 6811’s departure from expectations, illustrated in Figure 5. The rapid rise in P_{rot} from the late-F dwarfs to the early G dwarfs is well represented by the 1 Gyr Praesepe projection. By contrast,

the NGC 6811 sequence appears to diverge at redder colors and approach the Praesepe sequence. The natural conclusion is that K dwarfs have a lower braking index.

This challenge to the picture of a color-independent n is not unexpected: Angus et al. (2015) found that NGC 6811 and Praesepe had color dependencies that were different from each other and from the Hyades and Coma Ber clusters, leading these authors to discard the NGC 6811 and Praesepe samples from their calibration sample. Angus et al. (2015) speculated that these fitting problems could indicate limitations in the gyrochronology formula, and listed metallicity as a possible factor.

Agüeros et al. (2018) suggested an alternative scenario based on the results for NGC 752, whose age of 1.4 Gyr makes it significantly older than NGC 6811 and Praesepe. Agüeros et al. (2018) found that five mid-K dwarfs in the cluster had barely spun down compared to their cousins in Praesepe, while the three late-K/early M dwarfs had not slowed at all.⁹ Agüeros et al. (2018) hypothesized that stars enter a temporary phase of reduced net braking efficiency, where the stars stop spinning down. Based on where the NGC 6811 and NGC 752 color- P_{rot} sequences merged together with Praesepe’s, Agüeros et al. (2018) inferred that the duration of the stalling epoch must depend on mass, and last longer for lower-mass stars.

This work led us to predict that if the color- P_{rot} sequence for NGC 6811 were extended to lower masses, it would eventually merge with Praesepe’s. Indeed, as shown in Figure 5, NGC 6811’s deviation away from the 1 Gyr projection continues until $T_{\text{eff}} \approx 4295$ K (K6V), where it clearly overlaps with Praesepe. The late-K dwarfs of NGC 6811 have not spun down at all over the ≈ 350 Myr separating the two clusters.

This conclusion is even more striking when data for a younger cluster are included. The left panel of Figure 7 shows P_{rot} for the Pleiades (125 Myr; Rebull et al. 2016), Praesepe (Douglas et al. 2017, 2019), and NGC 6811. The Pleiades K dwarfs with $4500 < T_{\text{eff}} < 5000$ K have slowed down appreciably by 670 Myr (stars cooler than 4500 K yet converged on the slow sequence). However, the NGC 6811 stars in this same temperature range have hardly spun down relative to Praesepe, and the late-K/early M dwarfs have not spun down at all, despite their large difference in age.

The right panel of Figure 7 shows gyrochronology ages for individual stars in NGC 6811. While the G dwarfs

⁹ Agüeros et al. (2018) reported rotation periods for 12 stars in NGC 752. Four of these have *Gaia* DR2 astrometry and/or photometry inconsistent with single-star membership, and so we discarded them for the present discussion.

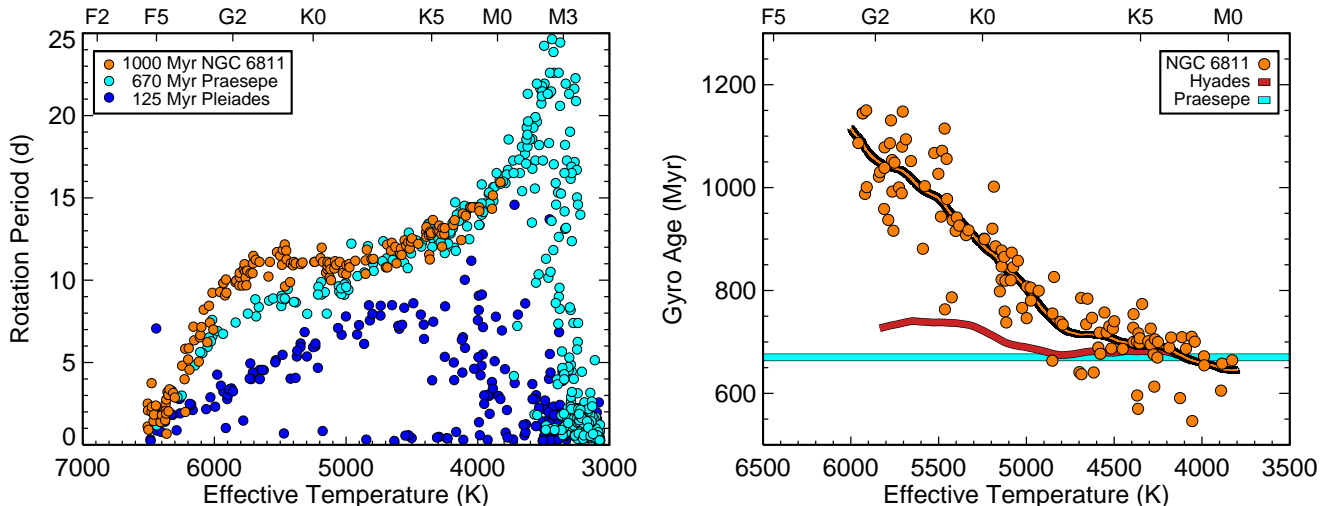


Figure 7. *Left*—The effective temperature–period distributions for the Pleiades (blue points, 125 Myr; [Rebull et al. 2016](#)), Praesepe (cyan points, 670 Myr; [Douglas et al. 2017, 2019](#)), and NGC 6811 (orange points). While stars in the Pleiades hotter than ≈ 4000 K have clearly spun down by the age of Praesepe, those cooler than 5000 K appear to stall between the age of Praesepe and that of NGC 6811. *Right*—The differential gyrochronology ages for NGC 6811 rotators (orange points) compared to our fiducial Praesepe model (cyan horizontal line; 670 Myr). We also include the LOWESS regression for the age difference (black–orange line), showing that the difference in gyrochronology ages is strongest for G stars, and decreases between $5250 > T_{\text{eff}} > 4700$ K until the cooler stars appear coeval with Praesepe. The same analysis for the Hyades relative to Praesepe ([Douglas et al. 2019](#)) is shown as the red curve.

show that the cluster is clearly older than Praesepe (represented by the cyan horizontal line at 670 Myr), this difference in age between NGC 6811 and Praesepe appears to vanish at $T_{\text{eff}} \lesssim 4700$ K.

3.3. Validating the stalled braking scenario with *Kepler*

While in models n is generally taken to be independent of color and constant in time (e.g., [Barnes 2007](#)), data like those presented in Figure 5 have been used to suggest that K dwarfs spin down more gradually than their more massive siblings. For example, comparing the P_{rot} sequences of M34 and NGC 6811 to that for the Hyades led [Meibom et al. \(2011a,b\)](#) to suggest that n depends on color and is smaller for redder/cooler stars.

We test this hypothesis by calculating a color-dependent braking index using our data for NGC 6811 and our empirical fit to Praesepe: if $P_{\text{rot}} \propto t^n$, then $n = \log(P_{\text{rot},2}/P_{\text{rot},1})/\log(t_2/t_1)$. We adopt ages for Praesepe and NGC 6811 of 670 Myr and 1 Gyr, and $A_V = 0.035$ and 0.15, respectively. The resulting dependence of n on DR2 color is shown in Figure 8. By eye, it seems that n is \approx constant for $(G_{\text{BP}} - G_{\text{RP}})_0 < 0.9$, after which it drops down toward 0.

It appears that the NGC 6811 data support a reduced braking efficiency for K dwarfs. However, this explanation cannot be correct, as we show by testing this model with the *Kepler* P_{rot} distribution for field stars ([McQuillan et al. 2014](#)). We propagate the Praesepe color– P_{rot}

sequence forward in time, assuming a color-dependent n , and compare the results to the observed distribution of P_{rot} . The bottom panel of Figure 8 shows the *Kepler* P_{rot} as a function of T_{eff} , along with the fit for Praesepe and the prediction for the approximate age of the Universe, 13.7 Gyr. According to this model, the Universe is not old enough for the K dwarfs in the *Kepler* field to have spun down to their observed $P_{\text{rot}} \approx 30$ –40 d.

We therefore interpret the data in the left panel of Figure 7 differently. Following the [Agüeros et al. \(2018\)](#) hypothesis, we argue that spin-down stalls after stars converge on the slow sequence for some amount of time, after which stars resume braking as expected with a common n . The shape of the curve in the right panel of Figure 7 reveals how the duration of stalling increases toward lower masses and cooler T_{eff} .

4. CONCLUSIONS

Prior to this work, the sample of rotators in the 1-Gyr-old cluster NGC 6811 was limited to 71 RV-confirmed members with masses $\gtrsim 0.8 M_{\odot}$. Fortunately, many more candidate members were targeted for observation for the *Kepler* Cluster Study ([Meibom et al. 2011b](#)).

We used data from *Gaia* DR2 to identify hundreds more likely single members with *Kepler* light curves, and we measured rotation periods for 171 of them. This more than doubles the size of the rotator sam-

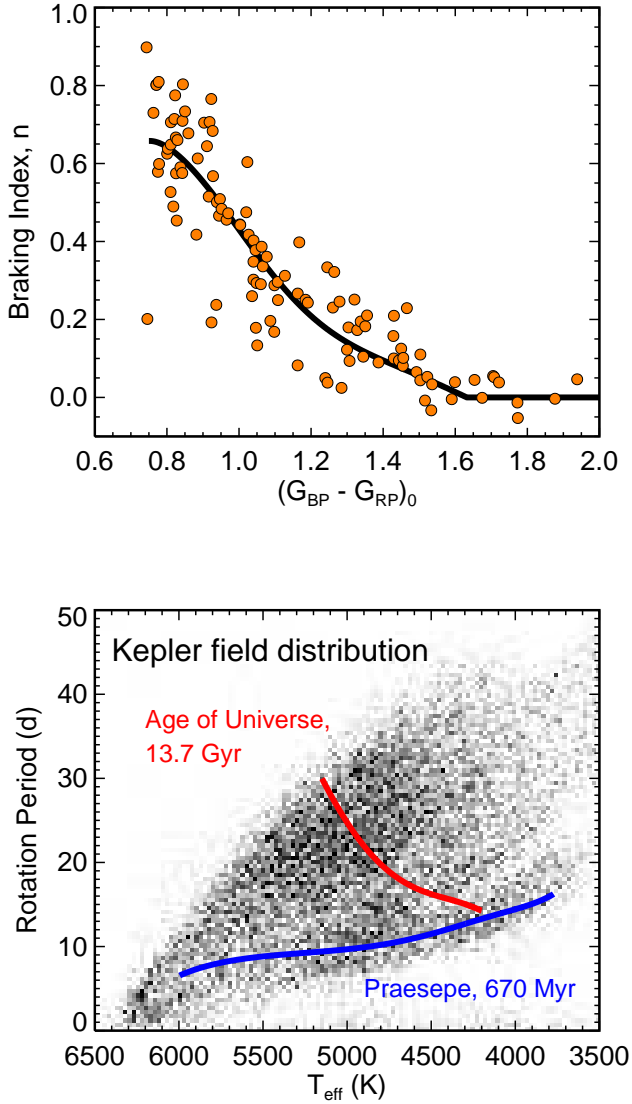


Figure 8. *Top*—The braking index n is calculated for NGC 6811 stars relative to Praesepe as a function of color. This plot could be interpreted as showing that spin-down depends on color. *Bottom*—The *Kepler* P_{rot} distribution (McQuillan et al. 2014) is plotted along with the Praesepe fit (670 Myr, blue line), and a 13.7 Gyr model created by projecting the Praesepe fit forward with the n from the top panel (red line). Clearly, a color-dependent braking law tuned with Praesepe and NGC 6811 cannot explain the observed *Kepler* P_{rot} distribution. The Universe is not old enough for those K dwarfs to have spun down to $P_{\text{rot}} \approx 30$ –40 d. The model is only plotted for K dwarfs, since more massive stars have lifetimes less than the age of the Universe.

ple for this cluster, and importantly extends it down to $M_{\star} \approx 0.6 M_{\odot}$, covering the full K dwarf range.

Focusing on the G dwarfs, for which we expect the Skumanich Law to be valid at least up to the age of the Sun (van Saders et al. 2016), we find an extremely precise gyrochronological age of $t_{\text{gyro}} = 1.04 \pm 0.07$ Gyr (median and standard deviation of 27 G-type stars), relative to the 670-Myr-old benchmark Praesepe (i.e., $\approx 1.5\times$ older). However, this difference in age appears to vanish for stars cooler than $T_{\text{eff}} < 4800$ K.

This could be interpreted as evidence for a mass-dependent braking index n , resulting in K dwarfs spinning down much more slowly than F and G dwarfs. However, this scenario cannot reproduce the distribution of $P_{\text{rot}} \approx 30$ –40 d observed for these stars in the *Kepler* field by McQuillan et al. (2014)—the Universe is not old enough for K dwarfs to spin down to these P_{rot} under this model.

Instead, we argue that K dwarfs stop spinning down after converging on the slow sequence at some time prior to the age of Praesepe. Braking stalls for an extended period of time, the duration of which increases toward lower masses/cooler temperatures. At some age older than NGC 6811 (1 Gyr) or NGC 752 (1.4 Gyr), the braking efficiency increases to a Skumanich-like value, and the stars resume spinning down.

What might be causing this epoch of stalled braking? The cluster data demonstrate that the net angular-momentum loss is low during this phase compared to the time before and following it. If this is the case, then either the braking torque is temporarily reduced, and/or the photosphere is gaining angular momentum from the interior to offset that lost via magnetic braking (e.g., Hartman et al. 2010; Denissenkov et al. 2010; Bouvier 2008; Gallet & Bouvier 2013, 2015; Lanzafame & Spada 2015).

Denissenkov et al. (2010) discuss a core–envelope decoupling model, and quote a timescale of $\tau_{\text{c-e}} = 55 \pm 25$ Myr and 175 ± 25 Myr for $1.0 M_{\odot}$ and $0.8 M_{\odot}$ stars ($T_{\text{eff}} \approx 4850$ K, K2). This K dwarf timescale does not seem long enough to address the spin-down discrepancy we see between NGC 6811 and Praesepe. Gallet & Bouvier (2015) quote values of $\tau_{\text{c-e}} = 150$ –500 Myr for $0.5 M_{\odot}$ stars, but their slowest track is only $\approx 70\%$ the period of Praesepe’s converged slow sequence, so modeling challenges persist. We are eager to see these theoretical models recalibrated with our new rotator sample for NGC 6811.

We propose that measurements of rotation in an even older cluster, for example, Ruprecht 147 (2.5 Gyr; Torres et al. 2018; Curtis 2016; Curtis et al. 2013), will show that the K dwarfs resume spinning down more efficiently

after the age of NGC 6811 or NGC 752, and we expect that the braking index that is found will be consistent with the distribution of P_{rot} observed in the *Kepler* field.

J.L.C. is supported by the National Science Foundation Astronomy and Astrophysics Postdoctoral Fellowship under award AST-1602662 and the National Aeronautics and Space Administration under grant NNX16AE64G issued through the *K2* Guest Observer Program (GO 7035). M.A.A. acknowledges support provided by the NSF through grant AST-1255419. S.T.D. acknowledges support provided by the NSF through grant AST-1701468. We thank Jennifer van Saders and Florian Gallet for sharing angular momentum evolution models (van Saders & Pinsonneault 2013; Gallet & Bouvier 2015), and the anonymous referee for providing a helpful and thorough review of this manuscript.

This paper includes data collected by the *Kepler* and *K2* missions, which are funded by the NASA Science

Mission directorate. We obtained these data from the Mikulski Archive for Space Telescopes (MAST). STScI is operated by the Association of Universities for Research in Astronomy, Inc., under NASA contract NAS5-26555. Support for MAST for non-HST data is provided by the NASA Office of Space Science via grant NNX09AF08G and by other grants and contracts.

This work has made use of data from the European Space Agency (ESA) mission *Gaia*,¹⁰ processed by the *Gaia* Data Processing and Analysis Consortium (DPAC,¹¹). Funding for the DPAC has been provided by national institutions, in particular the institutions participating in the *Gaia* Multilateral Agreement.

This research has also made use of NASA’s Astrophysics Data System, and the VizieR (Ochsenbein et al. 2000) and SIMBAD (Wenger et al. 2000) databases, operated at CDS, Strasbourg, France.

Facilities: Gaia, Kepler

Software: The IDL Astronomy User’s Library (Landsman 1993)

REFERENCES

- Agüeros, M. A., Bowsher, E. C., Bochanski, J. J., et al. 2018, *ApJ*, 862, 33
- Andrae, R., Foesneau, M., Creevey, O., et al. 2018, *A&A*, 616, A8
- Angus, R., Aigrain, S., Foreman-Mackey, D., & McQuillan, A. 2015, *MNRAS*, 450, 1787
- Anthony-Twarog, B. J., Deliyannis, C. P., & Twarog, B. A. 2014, *AJ*, 148, 51
- Bailer-Jones, C. A. L., Andrae, R., Arcay, B., et al. 2013, *A&A*, 559, A74
- Barnes, S. A. 2003, *ApJ*, 586, 464
- . 2007, *ApJ*, 669, 1167
- Basri, G., Borucki, W. J., & Koch, D. 2005, *NewAR*, 49, 478
- Bouvier, J. 2008, *A&A*, 489, L53
- Boyajian, T. S., von Braun, K., van Belle, G., et al. 2012, *ApJ*, 757, 112
- Brandt, T. D., & Huang, C. X. 2015, *ApJ*, 807, 24
- Bressan, A., Marigo, P., Girardi, L., et al. 2012, *MNRAS*, 427, 127
- Brewer, J. M., Fischer, D. A., Valenti, J. A., & Piskunov, N. 2016, *ApJS*, 225, 32
- Cardelli, J. A., Clayton, G. C., & Mathis, J. S. 1989, *ApJ*, 345, 245
- Cargile, P. A., James, D. J., & Jeffries, R. D. 2010, *ApJL*, 725, L111
- Cargile, P. A., James, D. J., Pepper, J., et al. 2014, *ApJ*, 782, 29
- Chen, Y., Girardi, L., Bressan, A., et al. 2014, *MNRAS*, 444, 2525
- Curtis, J. L. 2016, PhD thesis, Penn State University
- Curtis, J. L., Wolfgang, A., Wright, J. T., Brewer, J. M., & Johnson, J. A. 2013, *AJ*, 145, 134
- Denissenkov, P. A., Pinsonneault, M., Terndrup, D. M., & Newsham, G. 2010, *ApJ*, 716, 1269
- Douglas, S. T., Agüeros, M. A., Covey, K. R., et al. 2016, *ApJ*, 822, 47
- Douglas, S. T., Agüeros, M. A., Covey, K. R., & Kraus, A. 2017, *ApJ*, 842, 83
- Douglas, S. T., Curtis, J. L., Agüeros, M. A., et al. 2019, arXiv e-prints, arXiv:1905.06736
- Evans, D. W., Riello, M., De Angeli, F., et al. 2018, *A&A*, 616, A4
- Gaia Collaboration, Brown, A. G. A., Vallenari, A., et al. 2018a, *A&A*, 616, A1
- Gaia Collaboration, Babusiaux, C., van Leeuwen, F., et al. 2018b, *A&A*, 616, A10
- Gallet, F., & Bouvier, J. 2013, *A&A*, 556, A36
- . 2015, *A&A*, 577, A98
- Green, G. M., Schlafly, E. F., Finkbeiner, D., et al. 2018, *MNRAS*, 478, 651

¹⁰ <https://www.cosmos.esa.int/gaia>

¹¹ <https://www.cosmos.esa.int/web/gaia/dpac/consortium>

- Hartman, J. D., Bakos, G. Á., Kovács, G., & Noyes, R. W. 2010, *MNRAS*, 408, 475
- Herschel, J. F. W. 1833, *Philosophical Transactions of the Royal Society of London*, 123, 359
- Janes, K., Barnes, S. A., Meibom, S., & Hoq, S. 2013, *AJ*, 145, 7
- Kraus, A. L., & Hillenbrand, L. A. 2007, *AJ*, 134, 2340
- Landsman, W. B. 1993, in *Astronomical Society of the Pacific Conference Series*, Vol. 52, *Astronomical Data Analysis Software and Systems II*, ed. R. J. Hanisch, R. J. V. Brissenden, & J. Barnes, 246
- Lanzafame, A. C., & Spada, F. 2015, *A&A*, 584, A30
- Law, N. M., Kulkarni, S. R., Dekany, R. G., et al. 2009, *PASP*, 121, 1395
- Mann, A. W., Feiden, G. A., Gaidos, E., Boyajian, T., & von Braun, K. 2015, *ApJ*, 804, 64
- McQuillan, A., Mazeh, T., & Aigrain, S. 2014, *ApJS*, 211, 24
- Meibom, S., Barnes, S. A., Platais, I., et al. 2015, *Nature*, 517, 589
- Meibom, S., & Mathieu, R. D. 2005, *ApJ*, 620, 970
- Meibom, S., Mathieu, R. D., & Stassun, K. G. 2007, *ApJL*, 665, L155
- Meibom, S., Mathieu, R. D., & Stassun, K. G. 2009, *ApJ*, 695, 679
- Meibom, S., Mathieu, R. D., Stassun, K. G., Liebesny, P., & Saar, S. H. 2011a, *ApJ*, 733, 115
- Meibom, S., Barnes, S. A., Latham, D. W., et al. 2011b, *ApJL*, 733, L9
- Morris, B. M., Curtis, J. L., Douglas, S. T., et al. 2018, *AJ*, 156, 203
- Ochsenbein, F., Bauer, P., & Marcout, J. 2000, *A&AS*, 143, 23
- Press, W. H., & Rybicki, G. B. 1989, *ApJ*, 338, 277
- Rau, A., Kulkarni, S. R., Law, N. M., et al. 2009, *PASP*, 121, 1334
- Rebull, L. M., Stauffer, J. R., Bouvier, J., et al. 2016, *AJ*, 152, 113
- Sandquist, E. L., Jessen-Hansen, J., Shetrone, M. D., et al. 2016, *ApJ*, 831, 11
- Scargle, J. D. 1982, *ApJ*, 263, 835
- Skumanich, A. 1972, *ApJ*, 171, 565
- Smith, J. C., Stumpe, M. C., Van Cleve, J. E., et al. 2012, *PASP*, 124, 1000
- Soderblom, D. R. 2010, *ARA&A*, 48, 581
- Stumpe, M. C., Smith, J. C., Van Cleve, J. E., et al. 2012, *PASP*, 124, 985
- Torres, G., Curtis, J. L., Vanderburg, A., Kraus, A. L., & Rizzuto, A. 2018, *ApJ*, 866, 67
- van Saders, J. L., Ceillier, T., Metcalfe, T. S., et al. 2016, *Nature*, 529, 181
- van Saders, J. L., & Pinsonneault, M. H. 2013, *ApJ*, 776, 67
- Wenger, M., Ochsenbein, F., Egret, D., et al. 2000, *A&AS*, 143, 9

Table 1. Data for the NGC 6811 Benchmark Sample

#	KIC ID	<i>Gaia</i> DR2 Source ID	<i>G</i> (mag)	$(G_{BP} - G_{RP})$ (mag)	T_{eff} (K)	Mass (M_{\odot})	SpT	P_{rot} (d)	σP_{rot} (d)	N_Q	Code
1	9716563	2128134824634071424	13.313	0.569	6507	1.287	F5	1.11	0.3380	15	Y
2	9716076	2128122008451548672	13.350	0.570	6506	1.287	F5	2.50	0.0040	15	Y
3	9718403	2080469827339292672	13.444	0.574	6504	1.286	F5	2.09	0.3015	15	Y
4	9715923	2128125135187725696	13.337	0.580	6501	1.284	F5	0.92	0.0006	15	Y
5	9716858	2128133789541221888	13.581	0.607	6477	1.271	F5	3.74	0.5527	15	Y
6	9777642	2128137229815871232	13.547	0.608	6476	1.270	F5	2.01	0.2010	15	Y
7	9716139	2128145506212004608	13.435	0.609	6474	1.269	F5	2.31	0.3108	14	Y
8	9898009	2128518829068874112	13.702	0.619	6462	1.263	F5	1.44	0.1338	15	Y
9	9654924	2128121561774912128	13.635	0.622	6458	1.260	F5	1.83	0.1558	15	Y
10	9655708	2128131216861127680	13.665	0.631	6445	1.253	F5	2.38	0.3009	15	Y
11	9655437	2128132728689966720	13.812	0.652	6409	1.240	F5	1.38	0.0767	15	Y
12	9655357	2128108951750969088	13.722	0.658	6398	1.236	F5	1.81	0.1239	15	Y
13	9655145	2128121080738614016	13.905	0.670	6374	1.228	F5	1.49	0.0025	15	Y
14	9594739	2128107714800080384	13.891	0.671	6370	1.227	F5	2.22	0.1145	15	Y
15	9469799	2128018963596952832	13.896	0.672	6370	1.227	F5	2.49	0.1439	15	Y
16	9655730	2128131216861484928	13.895	0.672	6369	1.226	F5	2.06	0.0787	15	Y
17	9594038	2128118057081550464	13.944	0.674	6365	1.225	F5	1.90	0.0528	15	Y
18	9716253	2128144857677611264	13.931	0.674	6365	1.225	F5	2.75	0.2470	15	Y
19	9716817	2128133450244545024	13.801	0.675	6363	1.224	F5	0.67	0.3636	15	Y
20	9777089	2128141524783121792	14.000	0.678	6356	1.222	F5	3.21	0.1883	15	Y
21	9655727	2128132075854976896	13.975	0.681	6350	1.220	F5	3.03	0.1512	15	Y
22	9591888	2128077168993658624	14.012	0.681	6350	1.220	F5	3.03	0.1512	15	Y
23	9715848	2128124585431880704	13.959	0.682	6348	1.220	F5	2.04	0.0204	9	Y
24	9655716	2128132075854974336	14.072	0.685	6340	1.217	F5	3.37	0.2665	12	Y
25	9655385	2128109123549687680	14.035	0.698	6312	1.208	F8	3.15	0.1494	15	Y
26	9595079	2128127265491233280	14.132	0.703	6300	1.203	F8	2.87	0.0948	6	Y
27	9656480	2080097058538601088	14.318	0.725	6244	1.185	F8	4.81	0.1290	15	Y
28	9533215	2128103179314615296	14.154	0.732	6226	1.179	F8	3.98	0.2602	9	Y
29	9655911	2128128742959981312	14.228	0.734	6222	1.177	F8	5.83	0.5253	15	Y
30	9716376	2128144960756839424	14.207	0.734	6221	1.177	F8	1.99	0.0587	15	Y
31	9716401	2128145098195807872	14.205	0.742	6199	1.170	F8	5.18	0.4928	15	Y
32	9655282	2128108539434091392	14.370	0.743	6195	1.168	F8	5.86	0.2411	6	Y
33	9775854	2128126165979845376	14.278	0.746	6189	1.166	F8	4.56	0.1771	10	Y
34	9715126	2128165817117806464	14.297	0.756	6159	1.156	F8	7.18	0.6759	4	Y
35	9656016	2128130426587581440	14.459	0.759	6153	1.153	F8	6.35	0.3323	13	Y
36	9593926	2128119190952918016	14.324	0.771	6118	1.141	F8	5.05	0.2858	9	Y
37	9471344	2128098849987500160	14.515	0.774	6110	1.138	G0	6.53	0.3318	15	Y
38	9716435	2128144926397113728	14.525	0.775	6106	1.137	G0	6.67	0.2010	9	Y

Table 1 continued

Table 1 (*continued*)

#	KIC ID	<i>Gaia</i> DR2 Source ID	G (mag)	$(G_{BP} - G_{RP})$ (mag)	T_{eff} (K)	Mass (M_{\odot})	SpT	P_{rot} (d)	σP_{rot} (d)	N_Q	Code
39	9655268	2128120908939932032	14.520	0.778	6098	1.134	G0	7.15	0.4493	15	Y
40	9776415	2128145957189232256	14.562	0.784	6080	1.128	G0	8.21	0.6122	15	Y
41	9532828	2128102526479557248	14.528	0.793	6053	1.118	G0	6.23	0.3795	15	Y
42	9777258	2128140425271501824	14.692	0.797	6040	1.114	G0	8.45	0.1832	10	Y
43	9776409	2128151008070805888	14.709	0.799	6034	1.112	G0	7.42	0.3478	5	Y
44	9778187	2080475084380577152	14.795	0.806	6014	1.105	G0	9.23	0.4286	15	Y
45	9410241	2128096616604445312	14.679	0.808	6008	1.104	G0	7.00	0.1357	15	Y
46	9776475	2128146472585332096	14.857	0.825	5957	1.089	G0	9.28	0.6038	15	Y
47	9534045	2080086338300220032	14.904	0.833	5932	1.081	G2	9.82	0.5624	15	Y
48	9656165	2128130186069010944	14.892	0.833	5931	1.081	G2	9.82	0.5394	15	Y
49	9655917	2128131869696568960	14.899	0.837	5919	1.077	G2	9.08	0.2432	15	Y
50	9411496	2080057785357418240	14.949	0.840	5912	1.075	G2	10.04	0.4641	14	Y
51	9530806	2128068853937057408	15.030	0.841	5909	1.074	G2	9.24	...	1	Y
52	9594287	2128106477849445248	14.904	0.863	5840	1.056	G2	9.88	0.4857	15	Y
53	9716008	2128145785390512896	15.004	0.865	5833	1.054	G2	9.98	0.4072	15	Y
54	9655424	2128108676873069952	14.915	0.873	5810	1.049	G5	9.68	0.3383	15	Y
55	9532127	2128111975407524480	15.072	0.873	5808	1.049	G5	10.19	0.3753	15	Y
56	9592579	2128072564788836096	15.049	0.873	5807	1.048	G5	10.44	0.6905	15	Y
57	9470987	2128099670319729408	15.169	0.880	5786	1.044	G5	9.68	0.1934	15	Y
58	9655315	2128120840220460544	15.101	0.883	5777	1.042	G5	10.67	0.3633	15	Y
59	9716650	2128134549756166272	15.190	0.885	5771	1.040	G5	10.97	0.4127	15	Y
60	9715987	2128122283329454208	15.141	0.887	5765	1.039	G5	10.53	0.2703	15	Y
61	9655276	2128120702781491072	15.049	0.888	5763	1.038	G5	10.15	0.2139	15	Y
62	9716502	2128132694330246144	15.124	0.890	5757	1.036	G5	9.69	0.3416	15	Y
63	9776546	2128148018773587200	15.127	0.892	5751	1.034	G5	10.58	0.5511	15	Y
64	9836149	2128198836827103616	15.147	0.900	5725	1.027	G5	10.41	0.3628	15	Y
65	9896700	2128152760418078592	15.181	0.905	5710	1.022	G5	10.43	0.2606	15	Y
66	9716955	2128133518964049920	15.260	0.906	5707	1.021	G5	11.03	0.4030	15	Y
67	10018969	2128527487723005184	15.278	0.907	5704	1.020	G5	11.48	0.5578	15	Y
68	9777828	2128138054449629824	15.277	0.913	5686	1.015	G5	11.24	0.3175	15	Y
69	9838036	2128142933532501376	15.261	0.916	5675	1.012	G5	13.26	0.7145	13	S
70	9095289	2127962819783332608	15.287	0.917	5673	1.011	G5	13.56	0.8035	15	S
71	9718106	2080095615429775360	15.325	0.922	5657	1.006	G8	11.11	0.2655	15	Y
72	9593885	2128119087873695232	15.201	0.944	5589	0.986	G8	10.22	0.4332	15	Y
73	9655172	2128120256104862464	15.413	0.948	5578	0.983	G8	11.11	0.2305	15	Y
74	9838215	2128139600637881472	15.575	0.966	5524	0.969	G8	11.71	0.4624	15	Y
75	9531467	2128019994389145728	15.510	0.974	5501	0.963	G8	11.49	0.3041	15	Y
76	9957187	2128158601573673728	15.414	0.978	5486	0.959	G8	10.93	0.3486	15	Y
77	9776909	2128146713103563264	15.531	0.981	5480	0.958	G8	11.84	0.3286	12	Y
78	9656555	2080096886739921152	15.588	0.982	5477	0.957	G8	15.08	...	1	S

Table 1 continued

Table 1 (continued)

#	KIC ID	<i>Gaia</i> DR2 Source ID	<i>G</i> (mag)	(<i>G_{BP}</i> – <i>G_{RP}</i>) (mag)	<i>T</i> _{eff} (K)	Mass (<i>M</i> _⊙)	SpT	<i>P</i> _{rot} (d)	<i>σP</i> _{rot} (d)	<i>N</i> _Q	Code
79	9287620	2079958966750150272	15.632	0.985	5465	0.954	G8	12.17	...	1	Y
80	9469735	2128018379481370880	15.585	0.986	5464	0.954	G8	9.62	0.3344	15	Y
81	9471316	2128098746908279680	15.561	0.989	5454	0.951	G8	11.80	0.5301	15	Y
82	9777281	2128140253472804736	15.559	0.990	5451	0.950	G8	11.26	0.3377	14	Y
83	9776413	2128146335146361856	15.495	0.999	5425	0.944	G8	9.88	0.2627	15	Y
84	9655609	2128108024038073216	15.656	1.001	5420	0.943	G8	11.02	0.4898	15	Y
85	9656371	2080090667627204736	15.668	1.007	5402	0.938	K0	10.90	0.3827	15	Y
86	9654627	2128122420768295808	15.731	1.009	5396	0.937	K0	11.11	0.2504	14	Y
87	9595006	2128128055765212416	15.735	1.014	5382	0.933	K0	11.02	0.3848	15	Y
88	9469908	2128020166187804288	15.800	1.028	5343	0.923	K0	10.98	0.1800	14	Y
89	9469760	2128018826157984512	15.762	1.033	5330	0.920	K0	11.08	0.5434	15	Y
90	9716177	2128121218177579392	15.966	1.065	5241	0.898	K0	11.11	0.3808	14	Y
91	9838358	2128514053065223808	15.942	1.066	5238	0.897	K0	11.11	0.5126	13	Y
92	9716378	2128145304354240128	16.004	1.082	5193	0.887	K0	11.34	0.5629	13	Y
93	9655435	2128132586950838912	15.989	1.086	5185	0.885	K0	11.98	0.3800	14	Y
94	9654919	2128119671989269504	15.997	1.089	5175	0.883	K0	11.11	0.5609	14	Y
95	9654970	2128121561774914304	16.111	1.099	5151	0.877	K0	10.46	0.2355	15	Y
96	9837012	2128148671608654720	16.163	1.102	5141	0.875	K0	10.66	0.1761	14	Y
97	9286138	2128006662810036224	16.092	1.103	5141	0.875	K0	10.87	0.7441	15	Y
98	9655225	2128121012019139584	16.036	1.103	5140	0.875	K0	11.11	0.6488	15	Y
99	9655469	2128108814312039040	16.068	1.108	5126	0.872	K0	11.03	0.7185	15	Y
100	9594099	2128118916075039360	16.139	1.109	5123	0.871	K0	10.17	0.3487	14	Y
101	9835687	2128178976898255744	16.136	1.111	5119	0.870	K0	10.67	0.0330	3	Y
102	9775249	2128175334765924608	16.004	1.113	5114	0.869	K0	10.00	0.3087	10	Y
103	9655677	2128131418719632000	16.148	1.123	5089	0.863	K0	10.71	0.6440	15	Y
104	9654808	2128123069303321472	16.033	1.125	5083	0.862	K0	11.15	0.2196	13	Y
105	9836986	2128148568529429120	16.241	1.129	5075	0.860	K0	10.94	0.5297	14	Y
106	9777063	2128135408749666304	16.295	1.139	5048	0.854	K2	11.11	0.5649	13	Y
107	9594718	2128104141387273344	16.240	1.144	5038	0.852	K2	13.16	0.7599	13	S
108	9532052	2128112181565948800	16.172	1.149	5024	0.848	K2	10.44	0.2166	11	Y
109	9716694	2128134446676949120	16.027	1.160	4998	0.843	K2	10.37	0.6846	14	Y
110	9715637	2128124173114998272	16.106	1.161	4997	0.842	K2	10.90	0.5701	7	Y
111	9531975	2128111700529584000	16.293	1.170	4975	0.837	K2	10.99	0.1751	7	Y
112	9776327	2128149358803331840	16.245	1.171	4974	0.837	K2	10.78	0.1928	15	Y
113	9717373	2128135649267419904	16.425	1.190	4929	0.827	K2	11.18	0.2274	14	Y
114	9716302	2128144445360737408	16.468	1.225	4852	0.809	K2	10.39	0.1642	7	Y
115	9531969	2128111700529585024	16.526	1.225	4851	0.809	K2	11.20	0.4061	11	Y
116	9595731	2080089877353291136	16.521	1.230	4842	0.807	K2	11.85	0.5147	10	Y
117	9896609	2128158910811242496	16.593	1.247	4806	0.799	K2	11.28	0.3487	15	Y
118	9593995	2128118469398421632	16.638	1.253	4793	0.796	K2	11.29	0.1830	11	Y

Table 1 continued

Table 1 (*continued*)

#	KIC ID	<i>Gaia</i> DR2 Source ID	G (mag)	$(G_{BP} - G_{RP})$ (mag)	T_{eff} (K)	Mass (M_{\odot})	SpT	P_{rot} (d)	σP_{rot} (d)	N_Q	Code
119	9717161	2128136714419757952	16.694	1.262	4775	0.792	K2	13.11	0.5917	12	S
120	9716707	2128134618476431616	16.902	1.302	4698	0.774	K4	10.78	0.3101	11	Y
121	9838166	2128139497558660224	16.751	1.307	4688	0.772	K4	12.16	0.2646	7	Y
122	9657183	2080094000522047872	16.801	1.308	4686	0.772	K4	10.78	0.0073	2	Y
123	9655556	2128132488171813376	16.770	1.311	4681	0.771	K4	13.16	0.5852	11	S
124	9594399	2128108466414347264	16.840	1.323	4659	0.766	K4	11.79	0.4487	11	Y
125	9594079	2128118572477645824	16.813	1.327	4652	0.764	K4	12.27	0.4963	12	Y
126	9838228	2128139634997621376	16.863	1.341	4626	0.758	K4	12.02	0.1978	6	Y
127	9897654	2128144204842804992	16.904	1.347	4616	0.756	K4	11.02	0.0965	6	Y
128	9593626	2128116540951535744	16.871	1.362	4590	0.750	K4	11.61	0.1967	11	Y
129	9716918	2128133518964044032	16.910	1.366	4583	0.749	K4	11.92	0.8190	11	Y
130	9593890	2128119087873694208	16.760	1.369	4578	0.748	K4	11.53	0.1579	11	Y
131	9895567	2128179114337220608	17.001	1.383	4555	0.743	K4	12.43	0.3667	4	Y
132	9897050	2128155161299953024	16.975	1.390	4543	0.740	K4	12.10	0.2839	6	Y
133	9596065	2080085685465236864	16.908	1.400	4527	0.737	K4	12.30	0.1932	2	Y
134	9533430	2080064554225921792	17.054	1.407	4516	0.735	K4	11.91	0.2322	6	Y
135	9897078	2128155096879780736	17.033	1.413	4507	0.733	K4	12.35	0.2670	6	Y
136	9838655	2080477558281297152	17.138	1.418	4499	0.731	K4	12.54	0.0794	2	Y
137	9656681	2080095993386737408	17.183	1.449	4451	0.721	K5	12.21	0.1257	5	Y
138	9716678	2128134442376853120	17.334	1.484	4400	0.711	K5	18.83	0.4072	10	S
139	9716095	2128122004151549184	17.353	1.491	4391	0.709	K5	12.93	0.9576	10	Y
140	9471356	2128098884347245184	17.257	1.492	4390	0.708	K5	12.64	0.3280	6	Y
141	9593970	2128118228880232704	17.340	1.492	4389	0.708	K5	17.68	0.8943	4	S
142	9471158	2128098433369035392	17.394	1.492	4389	0.708	K5	13.22	0.0954	3	Y
143	9655970	2128130387927588992	17.322	1.506	4370	0.704	K5	12.74	0.3492	11	Y
144	9594642	2128107165044245888	17.297	1.507	4368	0.704	K5	11.55	0.2238	11	Y
145	9655566	2128132282013368960	17.119	1.511	4364	0.703	K5	11.26	0.6347	6	Y
146	9655067	2128120492322841728	17.404	1.512	4361	0.702	K5	12.95	0.1459	8	Y
147	9956996	2128208144016975488	17.313	1.517	4355	0.701	K5	12.76	...	1	Y
148	9470057	2128019307193856768	17.125	1.518	4353	0.701	K5	12.88	0.0759	2	Y
149	9655054	2128121389977163904	17.378	1.528	4340	0.698	K5	13.66	0.5414	6	Y
150	9897266	2128156673128579328	17.483	1.555	4305	0.689	K5	12.99	0.2186	5	Y
151	9530907	2128066998511354880	17.500	1.565	4292	0.686	K5	12.96	...	1	Y
152	9594284	2128108436354871936	17.565	1.566	4291	0.686	K5	13.32	0.4442	8	Y
153	9471304	2128098712548536320	17.398	1.572	4284	0.684	K5	10.87	...	1	R
154	9836401	2128197904814375808	17.471	1.579	4275	0.682	K5	12.79	0.3478	3	Y
155	9836918	2128151695265618944	17.564	1.582	4271	0.681	K5	12.04	0.3328	5	Y
156	9837294	2128153619411014400	17.558	1.585	4267	0.680	K5	13.16	0.3089	5	Y
157	9776201	2128149668040979456	17.611	1.596	4253	0.677	K5	12.79	...	1	Y
158	9593943	2128118327657867776	17.622	1.598	4250	0.676	K5	13.16	...	1	Y

Table 1 continued

Table 1 (*continued*)

#	KIC ID	<i>Gaia</i> DR2 Source ID	G	$(G_{BP} - G_{RP})$	T_{eff}	Mass	SpT	P_{rot}	σP_{rot}	N_{Q}	Code
			(mag)	(mag)	(K)	(M_{\odot})		(d)	(d)		
159	9656537	2080097195977577472	17.545	1.653	4185	0.660	K7	13.35	0.1459	3	Y
160	9533567	2080088537323743360	17.770	1.662	4175	0.658	K7	13.65	...	1	Y
161	9594614	2128107783519544448	17.813	1.706	4124	0.646	K7	12.44	...	1	Y
162	9895707	2128202410239878784	17.869	1.716	4114	0.643	K7	14.05	...	1	Y
163	9717490	2080097260396182016	17.945	1.737	4090	0.637	K7	13.91	0.0926	2	Y
164	9716651	2128134511096352640	18.135	1.768	4058	0.630	K7	14.43	...	1	Y
165	9656400	2128129632013326976	18.035	1.770	4055	0.629	K7	12.23	0.3799	5	Y
166	9716098	2128122042811294208	18.133	1.784	4041	0.626	K7	14.43	...	1	Y
167	9595606	2080089976131469568	18.220	1.835	3988	0.616	K7	14.43	...	1	Y
168	9836690	2128152068923234432	18.234	1.836	3987	0.616	K7	14.20	...	1	Y
169	9654921	2128119706349010944	18.365	1.933	3891	0.598	M0	14.34	...	1	Y
170	9655977	2128128910458794112	18.438	1.939	3885	0.597	M0	15.15	...	1	Y
171	9655330	2128108981810511616	18.377	2.001	3827	0.583	M0	15.96	...	1	Y
172	9837752	2128143478993406592	18.931	2.100	3740	0.558	M1	10.55	...	1	R

NOTE—The table is sorted according to $(G_{BP} - G_{RP})$, so also approximately by G . Effective temperature T_{eff} is calculated with an empirical color–temperature relation. P_{rot} is measured for every available Quarter between 2 and 16 with Lomb–Scargle periodograms. The standard deviation is adopted as the uncertainty, σP_{rot} . The number of Quarters of data used is N_{Q} . The code column denotes rapid (“R”), slow (“S”), and typical stars (“Y” for yes this is consistent with the cluster sequence).